

This document is confidential and is proprietary to the American Chemical Society and its authors. Do not copy or disclose without written permission. If you have received this item in error, notify the sender and delete all copies.

A new generation of ultrasensitive label-free optical Si nanowire-based biosensors

Journal:	<i>ACS Photonics</i>
Manuscript ID	Draft
Manuscript Type:	Article
Date Submitted by the Author:	n/a
Complete List of Authors:	<p>Irrera, Alessia; Istituto per i Processi Chimico-Fisici Consiglio Nazionale delle Ricerche, CNR Leonardi, Antonio; Università degli Studi di Catania Dipartimento di Fisica e Astronomia Di Franco, Cinzia; University of Bari, Dipartimento Interateneo di Fisica lo faro, Maria; Istituto per i Processi Chimico-Fisici Consiglio Nazionale delle Ricerche Palazzo, Gerardo; University of Bari, Department of Chemistry D'Andrea, Cristiano; CNR, IPCF Manoli, Kyriaki; University of Bari, Chemistry Franzo, Giorgia; CNR-IMM, MATIS, Dipartimento di Fisica e Astronomia Università di Catania Musumeci, Paolo; University, physics fazio, barbara; Istituto per i Processi Chimico-Fisici Consiglio Nazionale delle Ricerche Torsi, Luisa; University of Bari, Chemistry Priolo, Francesco; università di catania,</p>

SCHOLARONE™
Manuscripts

A new generation of ultrasensitive label-free optical Si nanowire-based biosensors

Alessia Irrera*¹, Antonio Alessio Leonardi^{1,2,3,4}, Cinzia Di Franco⁵, Maria Josè Lo Faro¹, G. Palazzo⁶, C. D'Andrea^{1,7}, Kyriaki Manoli⁵, Giorgia Franzò³, Paolo Musumeci², Barbara Fazio¹, Luisa Torsi*⁶, F. Priolo*^{2,3,8}.

1. IPCF-CNR, viale F. Stagno d'Alcontres 37, 98158 Messina, Italy.
2. Dipartimento di Fisica e Astronomia, Università di Catania, via S. Sofia 64, 95123 Catania, Italy.
3. MATIS IMM-CNR, via S. Sofia 64, 95123 Catania, Italy.
4. INFN, sezione di Catania, via S. Sofia 64, 95123 Catania, Italy.
5. CNR - Istituto di Fotonica e Nanotecnologie, Sede di Bari
6. Dipartimento di Chimica, Università degli Studi di Bari "Aldo Moro", via Orabona 4, 70126 Bari, Italy.
7. IFAC-CNR, Via Madonna del Piano, 10, I-50019 Sesto Fiorentino, Italy.
8. Scuola Superiore di Catania, Università di Catania, via Valdisavoia 9, 95123 Catania, Italy.

Keywords: Silicon, Nanowires, Bio-Sensor, Photoluminescence, C-Reactive Protein

* **corresponding authors:** Alessia Irrera, Luisa Torsi, Francesco Priolo.

Abstract

We demonstrate the realization of the first label-free optical biosensor based on the room temperature luminescence of silicon nanowires (NWs) tested for the selective detection of C-reactive protein in human serum. High aspect ratio Si NW arrays used as sensing interface, are synthesized by a fast, low-cost and Si industrially compatible approach. Si NW optical biosensors are fast and offer a broad concentration dynamic range that can be tuned according to different applications. Moreover, the platform is endowed with a high selectivity towards the target analyte and a sensitivity down to the fM limit of detection, opening the route towards non-invasive analysis in bio-fluids such as saliva.

Introduction

During the last decades the research community devoted a great deal of interest to the development of innovative sensing technologies for biological [1], clinical and environmental testing [2,3], as well as for energy storage and safety applications [4,5]. In this scenario, novel nanostructures arise as promising platforms for the realization of a new class of low cost and high performances biosensing devices due to their remarkable physical properties and the huge surface to-volume ratio that considerably enhance their potential in sensing applications. Silicon is the leading material for microelectronics and the realization of innovative sensing devices based on Si is of great interest for commercial applications. Several groups demonstrated the remarkable sensing performances of semiconducting quantum dots (QDs) [1,6], nanotubes (NTs) [7] and nanowires (NWs) [8] mainly by exploiting variations in their electrical conductivity [9,10].

Si NWs emerged in literature as the key materials for electrical sensing devices because of the huge amount of exposed surface as well as of their electrical conductivity being high compared to

1
2
3 other nanostructures [11]. Although several groups have already demonstrated detection limits in
4
5 the picomolar (pM) concentrations range by means of a single Si NW Field Effect Transistor
6
7 [12,13], the manufacturing of such devices is extremely complex, expensive and time-consuming.
8
9 Moreover, the control over the NW doping can be hardly obtained by conventional growth
10
11 processes. Conversely, the fabrication of electrical sensors with high density arrays of NWs is cost-
12
13 effective and scarcely reported.
14

15
16 The recent advancement in nanotechnology enables to surpass the electric transduction sensors
17
18 with label-free optical ones, achieving improved performances at a lower fabrication cost. Most of
19
20 the commercially available optical sensors, such as enzyme-linked immunoassay arrays (ELISA),
21
22 involve the interaction of the target analyte with a luminescent marker such as dyes, fluorophores,
23
24 emitting quantum dots, *etc.* [14]. The label characteristic optical emission, besides providing only
25
26 an indirect evidence for the presence of the analyte, degrades with time and exposure to the
27
28 environment, causing also information loss by photobleaching. Other quenching mechanisms can
29
30 occur also between labels, limiting the detection efficiency and the reliability of this kind of sensors
31
32 [15]. Moreover, such an indirect and non-specific targeting increases the detection noise, reducing
33
34 the performances of labeled sensors. In order to overcome these disadvantages a new class of label-
35
36 free optical biosensors is under current investigation and recent developments addressed the
37
38 emission quenching (or enhancement) of quantum confined nanostructures as a suitable sensing
39
40 mechanism [16]. These label-free optical sensors based on emitting nanostructures guarantee faster
41
42 and easier measurements relying on the direct and selective interaction of the functionalized
43
44 transducing interface and the target analyte. Along this line, bright and stable luminescence has
45
46 been demonstrated in quantum confined nanostructures whose emission wavelength can be tuned
47
48 with great accuracy by engineering the confinement dimension [17,18]. In particular, light emitting
49
50 quantum dots (QDs) composed of different materials have been proposed by many groups as
51
52 promising label-free optical biosensors based on either PL quenching or enhancement according to
53
54 the analyte/QD surface interaction [19]. The occurrence of non-radiative processes during the QD-
55
56
57
58
59
60

1
2
3 target interaction is responsible for the optical quenching of QD emission. For example, 1.1 μM
4
5 cyanide detection has been demonstrated by means of CdSe QDs modified with tert-butyl-n-(2-
6
7 mercaptoethyl)-carbamate [19]. Apparently, label-free QD optical sensors generally exhibit poor
8
9 detection limits falling in the nM – mM range [16,19]. Such low sensitivities limit the use of QDs
10
11 for practical applications in non-invasive assays requiring ultra-low sensitivity down to the pico and
12
13 femtomolar (fM) range [20-24]. While mostly II-IV QDs have been engaged so far, [25,26] it
14
15 should be noted that Se and Te are toxic and the use of heavy metal species (Pb, Cd, Zn) is
16
17 generally avoided in devices since they diffuse during the industrial processes, compromising the
18
19 device performances. Furthermore, it is extremely complex and inefficient to electrically excite QD
20
21 emission and, aside from optical pumping, their implementation in optoelectronic devices is
22
23 strongly limited.
24
25

26
27 Silicon is the leading material for industrial applications and the realization of innovative sensors
28
29 based on Si nanostructures, implementable with the current industrial technology, is attracting the
30
31 interest of the scientific community and is also strategic for commercial exploitation. Indeed, the
32
33 sensing potential of Si-based platforms has been investigated by many research groups due to its
34
35 biocompatibility, non-toxicity and availability at low cost. Nonetheless, room temperature emission
36
37 from Si is scarcely reported in literature due to its indirect bandgap and, hence, can only be
38
39 observed for quantum confined nanostructures such as Si QDs [27], porous Si [28] and most
40
41 recently from Si NWs [29,30].
42
43

44
45 Notably, 1D materials such as Si NWs provide higher aspect ratio, high exposed surface, easy
46
47 electrical pumping, robustness and high PL stability compared to QDs. Nevertheless, since their
48
49 optical emission has been achieved only recently, their implementation in optical biosensors is still
50
51 largely unexplored.
52
53

54
55 Indeed, the role of room temperature (RT) light emitting Si NWs is strategic for the optical
56
57 biosensing framework, opening the route towards the development of a new generation of ultra-
58
59 sensitive and low cost label-free optical sensors. In this respect, some of the authors already
60

1
2
3 demonstrated the realization of thin Si NWs synthesized by a low cost, fast and industrially
4 compatible approach, which demonstrated RT luminescence ascribable to quantum confinement
5 effect [31-33]. In this work we exploit the sensing response of these RT luminescent Si NW arrays
6 whose surface has been bio-functionalized for the selective detection of the C-Reactive protein
7 (CRP) over a wide dynamic concentration range. CRP is of crucial interest for the detection of a
8 wide variety of clinical pathologies since its presence at high concentration in blood vessels is
9 associated to the occurrence of acute inflammatory conditions, often associated with heart-failure
10 pathologies. More specifically, high level of CRP concentration above the standard value of 3 $\mu\text{g/ml}$
11 (25 nM) in blood serum, is related to a cardiovascular risk [34]. Cardiovascular problems are some
12 of the major cause of death for both men and women so the availability of high-sensitivity, low-cost
13 and reliable CRP sensors is a priority in clinical diagnostic [35]. The most accurate commercial
14 tests currently adopted, such as the ELISA one, already allow for the quantitative analysis of CRP
15 in blood serum. The ELISA test, however, being label needing, provides an indirect quantification
16 of CRP that is based on the colorimetric readout of the immunoassay and it is therefore limited only
17 to elevated CRP concentrations in the 10 – 20 $\mu\text{g/ml}$ (85 – 170 nM) range, exceeding the normal
18 reference level [36]. Moreover, this test produces false positive results for prolonged incubation
19 time since the color intensity can fade or saturate. Another crucial limitation of this clinical protocol
20 is related to the occurrence of nonspecific binding yielding to a high number of false positive
21 results. Finally, the assay is made in blood serum and it is typically performed within a hospital.
22 The possibility of direct CRP detection within extended concentration ranges, enabling also for non-
23 invasive testing, with a good reliability by using a sensing system that is easy to implement with the
24 industrial processes, is still scarcely reported.

25
26
27
28
29
30
31
32
33
34
35
36
37
38
39
40
41
42
43
44
45
46
47
48
49
50
51
52 In this work we demonstrate the high level of performances and the great potentialities of a new
53 generation of optical biosensors based on room temperature luminescent Si NW arrays realized at
54 low cost with an industrially compatible approach for the direct label-free CRP detection over a
55 broad range of concentrations with ultra-high-sensitivity and high selectivity. While the assay is
56
57
58
59
60

1
2
3 successfully bench-tested in human serum, the platform would prospectively allow for CRP
4
5 detection even in saliva opening the route towards sensors that enable non-invasive self-use even at
6
7 home.
8
9

10 11 **Results and Discussion**

12
13
14 High density ($\sim 10^{12}$ NW/cm²) arrays of vertically aligned silicon nanowires (Si NWs) were
15
16 prepared by metal assisted chemical etching (MACE) as described in the Methods. The cross
17
18 section scanning electron microscopy (SEM) image of a dense array of vertically aligned Si NWs
19
20 having length of about 3 μm is shown in Figure 1. The Si NWs are endowed with the needed
21
22 selectivity towards the CRP target analyte by means of an *ad-hoc* designed surface bio-
23
24 functionalization procedure comprising the steps presented in Figure 1(a-c), namely: at first
25
26 streptavidin (SA) proteins are physisorbed directly on the NWs surface. Afterwards, biotinylated
27
28 capturing anti-CRP antibodies (Ab) are let to bound to SA. As it is well known that the streptavidin-
29
30 biotin is one of the strongest non-covalent protein-ligand bond ($K_{\text{diss}} = 10^{15} \text{ M}^{-1}$) so as a very stable
31
32 anti-CRP capturing bio-layer forms on the NWs surface. Moreover, the biotin-streptavidin binding
33
34 is extremely rapid and once the complex is formed it is only weakly affected by external parameters
35
36 such as pH, temperature, organic solvents or denaturizing agents [37]. To enable the SA
37
38 physisorption, the Si NWs are immersed in a SA solution (Figure 1b) while for the attachment of
39
40 the anti-CRP antibody, the NWs are immersed in an biotinylated anti-CRP solution so as the Ab
41
42 stably binds to SA (Figure 1c). The incubation of the fully bio-functionalized NWs into a CRP
43
44 solution of a given concentration results in the binding of CRP with a very high degree of
45
46 selectivity (Figure 1d). More details are provided in the Methods section.
47
48
49
50
51

52
53 A key factor in the fabrication of a reliable sensor is the reproducible and uniform bio-
54
55 functionalization. As already anticipated, the bio-functionalization protocol chosen involves well
56
57 known, strong bonding between the streptavidin and the biotinylated anti-CRP. The interaction
58
59 between the streptavidin and the silica shell of the NWs relies, on the contrary, on usually weaker
60

1
2
3 physical interactions. Hence, the uniformity and the stability of this key important first bio-
4
5 functionalization step needs to be demonstrated. A confocal microscopy characterization of the SA-
6
7 functionalized Si NWs was therefore carried out. To endow the proteins of the needed fluorescent
8
9 capability, a fluorescent equivalent of SA, marked with the Alexa Fluor 488 fluorophore, (F-SA),
10
11 was engaged. The uniformity of the SA-functionalization was assessed both in-plane (x-y confocal
12
13 plane) and along the Si NW vertical profile (z-x confocal plane), and the results are show in Figure
14
15 2. Specifically, Figure 2a and 2b report in-plane and z-axis images of the pristine Si NWs emission
16
17 under an excitation of 405 nm (see Methods for details). The signal from the F-SA-functionalized
18
19 NWs, excited at 488 nm, is shown as a green in-plane and z-axis fluorescence in Figure 2c and 2d,
20
21 respectively. The F-SA functionalization is clearly uniform throughout the x-y-plane as well as
22
23 along the Si NW vertical profile as it can be appreciated from the expected yellow fluorescence
24
25 generated by the combinations emissions coming from the NWs and the F-SA layer (Figure 2e and
26
27 2f). Relevantly, despite the high aspect ratio of the Si NWs, a uniform SA-functionalization is
28
29 demonstrated both in-plane and along the vertical profile of the NWs. The stability of the SA
30
31 physisorbed layer was also demonstrated as the uniform SA-layer was persistent even after the
32
33 several washing steps foreseen throughout the whole bio-functionalization protocol.
34
35
36
37

38
39 The bio-functionalized, comprising both SA and anti-CRP, Si NWs were incubated in CRP
40
41 standard solutions at concentrations ranging from 10^{-9} $\mu\text{g/ml}$ to 100 $\mu\text{g/ml}$ (8.5 aM to 850 nM).
42
43 Importantly, the pH and the ionic strength of the CRP in phosphate buffer saline (PBS) solution are
44
45 comparable to those of real biological fluids such as blood serum. The PL spectra of the Si NW
46
47 sensor are plotted after incubation in CRP standard solution of increasing concentration (Figure 3).
48
49 The black spectrum is the emission of the pristine bio-functionalized Si NWs (without CRP) taken
50
51 as the base-line. The PL spectra of the NW sensors incubated at different CRP concentrations
52
53 (sensor signal at a given CRP concentration), show two PL peaks falling at about 510 nm and 700
54
55 nm. To experimentally de-convolve the two components in bio-functionalized Si NWs, the PL of
56
57 the SA-Ab complex onto a bare Si wafer (without NWs) as well as of the bare Si NWs PL were
58
59
60

1
2
3 compared, enabling to ascribe the 510 nm peaked emission to the SA-Ab complex and that around
4
5 700 nm to pristine Si NWs. The decrease of the PL intensities in the 600-800 nm range with respect
6
7 to the base-line is clearly visible for all the samples exposed to CRP. In fact, the quenching of the
8
9 NW PL intensity increases by increasing the CRP concentration. The PL spectra for CRP
10
11 concentrations of 10^{-9} and 10^{-8} $\mu\text{g/ml}$ (8.5 aM and 85 aM) show a relative difference of 17%
12
13 compared to the base-line (black spectrum) but it is not possible to distinguish between the signals
14
15 relevant to the two elicited concentrations. By increasing the CRP concentration by one order of
16
17 magnitude (10^{-7} $\mu\text{g/ml}$, 850 aM) a PL relative reduction of about 10% is recorded, and an additional
18
19 similar percentage reduction is observed up to CRP concentrations of 10^{-6} $\mu\text{g/ml}$ (8.5 fM). The
20
21 quenching of the PL intensity is attributed to the occurrence of non radiative phenomena associated
22
23 with the presence of the CRP on the surface of the NWs. To demonstrate the presence of such non
24
25 radiative phenomena, the lifetime τ of the NW sensor before (red line) and after exposure to a CRP
26
27 concentration of 10^{-7} $\mu\text{g/ml}$ (850 aM) (blue line) are given in the inset of Figure 3. The lifetime of
28
29 the base-line device (bare bio-functionalized NWs) is $\tau_{\text{SA-Ab}} = 25$ μs whereas the lifetime of the
30
31 NWs after exposure to CRP, decreases down to $\tau_{\text{CRP}} = 20$ μs . The lifetime reduction by a factor of
32
33 1.25 is comparable to that measured for the PL intensities of the same samples, demonstrating that
34
35 the non radiative phenomena are responsible for the PL quenching.
36
37
38
39
40
41

42 Indeed, the equation rate of the NW radiative de-excitation is:

$$\frac{dN^*}{dt} = \sigma\phi(N - N^*) - \frac{N^*}{\tau} \quad (1)$$

44
45
46
47
48 Where N^* is the number of the excited emitting centers, N is the total number of emitting centres, τ
49
50 is the total lifetime of the system, σ is the excitation cross section and ϕ is the photon flux. In the
51
52 stationary state equation (1) is equal to zero and in low excitation conditions it can be assumed that:
53
54 $\sigma\phi\tau \leq 1$, which leads to the following expression for N^* :
55
56
57
58
59
60

$$N^* = \frac{\sigma\phi\tau}{\sigma\phi\tau + 1} N \cong \sigma\phi\tau N \quad (2)$$

The PL intensity is equal to $I_{PL} \propto \frac{N^*}{\tau_{rad}}$, where τ_{rad} is the radiative lifetime, substituting equation (2)

the following expression is hence obtained:

$$I_{PL} \propto \frac{N^*}{\tau_{rad}} \cong \sigma\phi N \frac{\tau}{\tau_{rad}} \quad (3)$$

leading to the conclusion that I_{PL} is proportional to the overall lifetime of the system τ .

The measurement of the same attenuation factor for both I_{PL} and τ of the NWs is hence a strong demonstration that the non radiative phenomena introduced from the CRP binding are at the origin of the PL quenching. In order to correctly estimate the decrease of the PL intensity of Si NWs for the different CRP concentrations, the fitting curves of the PL spectra are calculated by considering both contributions at 510 nm and 700 nm. In particular, the spectra of the bare Si NWs (700 nm) and of SA-Ab complex (510 nm) are summed together and each one re-scaled in intensity to perfectly fit the bio-functionalized Si NWs curve. This is taken as the starting point. Both components are then re-scaled to properly fit the spectra measured at different CRP concentrations and the scaling factors for the NW component (at 700 nm) represents the normalized integrated PL Intensity. In Figure 4 the CRP dose curve built as the complement to 1 of the normalized NWs PL integrated peak intensity as a function of the CRP concentrations, is shown. The NW PL intensity at 10^{-9} and 10^{-8} $\mu\text{g/ml}$ (8.5 aM and 85 aM) of CRP set the level of the noise (0.11 ± 0.04 , the reproducibility error taken as one standard deviation). At higher concentrations, the PL signal decreases continuously and its complement increases until saturation is reached. Overall the sensing dose-curve spans a CRP concentration dynamic range as high as 7 orders of magnitude (from 10^{-8} to 1 $\mu\text{g/ml}$, 85 aM – 8.5 nM). In the linear range of the dose curve (from 10^{-8} to 10^{-3} $\mu\text{g/ml}$, 85 aM to

1
2
3 8.5 pM) the PL intensity decreases by 25%, while a further decrease is observed up to a
4
5 concentration of 1 $\mu\text{g/ml}$ (8.5 nM), above which saturation is reached.

6
7 The fitting of the calibration curve for CRP sensing shown in Figure 4 was performed using Hill's
8
9 binding model [38] given by:

$$y = V_{\max} \frac{x^n}{K_D^n + x^n} \quad (4)$$

10
11
12 where y is the response of the sensors, V_{\max} is the degree of saturation, x is the ligand concentration
13
14 (M), n shows the degree of cooperativity and K_D is the dissociation constant.

15
16
17 The fitting returned a dissociation constant $K_D = 8.3 \pm 2.3 \cdot 10^{-14}$ M and a plateau response at a
18
19 saturation $V_{\max} = 0.95 \pm 0.02$. The n was found to be equal to 0.29 which is < 1 , suggesting an anti-
20
21 cooperative binding for CRP. The computed limit of detection (LODs) was as low as 1.6 fM. Such
22
23 an ultralow sensitivity of the NW biosensor opens the route towards non invasive analysis in saliva
24
25 with a great advantage for the patient [20]. In fact, in literature a healthy adult patient presents an
26
27 average concentration of CRP in saliva well below 10^{-4} $\mu\text{g/ml}$ (850 fM), whereas the risk of
28
29 myocardial infarction is extremely high for those subjects presenting a CRP concentration in saliva
30
31 above 10^{-3} $\mu\text{g/ml}$ (8.5 pM) [20], whose detection would be enabled by the NW biosensors
32
33 technology here presented. These results demonstrate the enormous potentialities of Si NW
34
35 biosensors enabling the realization of a sensing device at low cost for the primary health care
36
37 diagnostic.

38
39
40 Critical at this point is to prove that the platform is capable of a high performance level also in real
41
42 samples such as blood serum. To this end, the serum of a human volunteer was spiked with a
43
44 concentration of 10^{-2} $\mu\text{g/ml}$ (85 pM) of CRP and tested. The PL intensity of the sensor incubated in
45
46 human serum, shown as a red-dot reported in Figure 4, is indeed very close to the PL response to
47
48 the same concentration of CRP in phosphate buffer solution (PBS), proving that CRP assay is
49
50 possible in a real sample. This was already encouraging, but also selectivity needed to be proved in
51
52
53
54
55
56
57
58
59
60

1
2
3 such a complex real-matrix. Hence, a negative control experiment was designed. To this end, the
4
5 NWs bearing the anti-CRP capturing antibody were incubated in PBS comprising bovine serum
6
7 albumin (BSA) instead of CRP proteins. BSA is known not to selectively bind to anti-CRP, indeed
8
9 no PL intensity significant variation respect to bio-functionalized NWs without BSA was observed
10
11 upon incubation in the BSA solution at concentrations ranging from 10^{-5} $\mu\text{g/ml}$ to 10 $\mu\text{g/ml}$. The
12
13 anti-CRP functionalized NWs selectivity was further challenged by changing the functionalization
14
15 protocol. In that, the same concentration of SA (10 $\mu\text{g/ml}$) was used but instead of the 50 $\mu\text{g/ml}$ of
16
17 Ab the same amount of BSA was used. By exposing to different CRP concentrations, no significant
18
19 variation of the PL intensities compared to the NWs functionalized with only SA and BSA are
20
21 measured confirming, as expected, that no binding of CRP to BSA occurs also in this case.
22
23

24
25 The detection on the 10^{-9} to 100 $\mu\text{g/ml}$ (8.5 nM to 850 nM) regimes very-well matches the typical
26
27 CRP concentration range for the early-diagnosis of heart attack in saliva and also allows to prove
28
29 the very low LODs that are enabled by the Si NW array. However the elicited low-concentration
30
31 range does not enable the detection of CRP in blood serum for the cardiovascular risk diagnosis,
32
33 which is the standard methodology clinically adopted today. Indeed, regarding cardiovascular
34
35 disease, a CRP level in blood serum lower than 1 $\mu\text{g/ml}$ (8.5 nM) is reported to indicate a low risk
36
37 of coronary syndrome, CRP between 1 and 3 $\mu\text{g/ml}$ (8.5 nM to 25 nM) points to an average risk,
38
39 between 3 and 10 $\mu\text{g/ml}$ (25 nM to 85 nM) to a high risk and a CRP concentration higher than 10
40
41 $\mu\text{g/ml}$ (85 nM) is typical of an acute coronary syndrome [39]. In the calibration curve reported in
42
43 Figure 4, saturation is observed for CRP concentrations higher than 1 $\mu\text{g/ml}$ (8.5 nM) and hence the
44
45 elicited ranges characterizing cardiovascular disease risk, are not accessible. To tailor the sensitivity
46
47 of the NW sensors for such CRP range in serum, the functionalization procedure was modified
48
49 using 20 $\mu\text{g/ml}$ of SA and 100 $\mu\text{g/ml}$ of Ab, doubling both the SA and Ab concentrations used in
50
51 the first functionalization protocol. The PL spectra for this dynamic range are reported in Figure 5,
52
53 showing the PL quenching already observed with increasing CRP concentration. The black line is
54
55
56
57
58
59
60

1
2
3 the PL spectrum after incubation of the bio-functionalized NW array in the bare PBS solution. The
4
5 sensing mechanism is also in this case, determined by the occurrence of the non radiative
6
7 phenomena introduced by the CRP bonding. In fact, the lifetime of the reference sensor incubated
8
9 only with SA and Ab is 20 μs while after the incubation in 10^{-2} $\mu\text{g/ml}$ (85 pM) of CRP it decreases
10
11 to 15.7 μs (as visible from the inset reported in Figure 5) with a factor which is the same to the one
12
13 measured from the corresponding integrated PL peak intensities. These results are in very good
14
15 agreement with the trend observed in the NWs bio-functionalized at lower SA/Ab concentrations
16
17 dynamic range (Figure 3), confirming that the PL quenching mechanism arises also in this case
18
19 from non radiative phenomena. Most importantly, the dynamic range from 1 to 10 $\mu\text{g/ml}$ (8.5 nM to
20
21 85 nM) is now clearly accessible for the detection. The PL intensities have been fitted by using the
22
23 same procedure previously adopted. The PL integrated peak of the NW sensor are reported as a
24
25 function of the CRP concentrations, as shown in Figure 6. This dynamic range is sensitive over four
26
27 orders of magnitude of CRP concentrations (from 10^{-2} to 100 $\mu\text{g/ml}$, 85 pM to 850 nM), perfectly
28
29 matching the critical CRP concentration range for cardiovascular risk in blood, as reported in
30
31 literature [39]. These results show the flexibility of the detection range of the NW sensors, in fact it
32
33 is now demonstrated that by changing the concentrations of the functionalization it is possible to
34
35 realize a sensor with tailored sensibility towards different concentration ranges. Figure 7 provides
36
37 the comparison between the dynamic detection ranges studied in this paper, showing that the PL
38
39 quenching is less pronounced in the second range with respect to the first one when the same value
40
41 of CRP concentration is considered. At a first glance this behavior might seem counterintuitive
42
43 since by increasing the capturing anti-CRP proteins the sensor becomes less sensitive. In order to
44
45 understand the whole set of data we hence explored also the opposite regime and decreased the SA
46
47 and Ab functionalizing solutions (by always maintaining the 1:5 ratio). In Figure 7 we also
48
49 provided some experimental measurements obtained by functionalizing the NWs with 1 $\mu\text{g/ml}$ of
50
51 SA and 5 $\mu\text{g/ml}$ of Ab (green dots). The quenching observed for the base-line (sensor without CRP)
52
53
54
55
56
57
58
59
60

1
2
3 in this configuration is 1.14 times lower with respect to the base-line corresponding to the 10 $\mu\text{g/ml}$
4 of SA and 50 $\mu\text{g/ml}$ of Ab functionalization, thus in spite of an order of magnitude difference, the
5 two sensors appear to be very similar. Indeed, the 1 $\mu\text{g/ml}$ of SA and 5 $\mu\text{g/ml}$ of Ab sensor (green
6 dots) has also a very similar PL trend to the 10 $\mu\text{g/ml}$ of SA and 50 $\mu\text{g/ml}$ of Ab one (blue dots) in
7 the whole inspected CRP concentrations range. These results strongly suggest that all the available
8 NW surface is hence already fully functionalized by using the low concentration functionalization.
9 Going to 10 $\mu\text{g/ml}$ of SA and 50 $\mu\text{g/ml}$ of Ab maintains the properties of the sensor identical.
10 Further increasing the SA/Ab content to 20 $\mu\text{g/ml}$ of SA and 100 $\mu\text{g/ml}$ of Ab has instead a strong
11 effect and the properties of the sensor are deteriorated, with a decrease in intensity by 25 % already
12 for the base-line. Since the anchoring sites are saturated it is now possible for SA proteins to bind
13 between themselves [40,41]. This will produce a reduction of the reference PL intensity. In
14 addition, anchoring sites for CRP will hence be far away from the NW surface and, as a
15 consequence there will be a reduced effect of CRP concentration on PL quenching, as observed.
16 While in principle this is a detrimental effect in fact, as shown, it can be advantageously used in
17 order to monitor high CRP concentrations. The optimization of the capturing layer shows that it is
18 possible to vary the dynamic detection range by optimizing the SA and capturing Ab concentrations
19 in the functionalization procedure. The 1 $\mu\text{g/ml}$ of SA and 5 $\mu\text{g/ml}$ of Ab functionalization solution
20 consents to functionalize the whole NW surface as similar results are obtained when the 10 $\mu\text{g/ml}$
21 of SA and 50 $\mu\text{g/ml}$ of Ab ratio is used.
22
23
24
25
26
27
28
29
30
31
32
33
34
35
36
37
38
39
40
41
42
43
44
45
46
47
48

49 **Conclusions**

50
51
52 The realization of a new class of luminescence biosensors based on Si nanowires for the C-reactive
53 protein is demonstrated. These sensors are based on the quenching of the PL signal at room
54 temperature due to the occurrence of non radiative phenomena introduced by the formation of the
55
56
57
58
59
60

1
2
3 biological complexes on the NW surface. By functionalizing the NWs with 10 $\mu\text{g}/\text{ml}$ of SA and 50
4 $\mu\text{g}/\text{ml}$ of Ab the limit of detection of 1.6 fM is demonstrated. Such a low value, opens the route
5
6 towards non invasive analysis in saliva strategic for health care diagnosis. Both quantification and
7
8 selectivity is demonstrated in human serum showing strong potentialities for the medical field. By
9
10 increasing the concentration of the capturing anti-body attached to the surface, CRP detection range
11
12 can be modulated to cover the 10^{-2} $\mu\text{g}/\text{ml}$ up to 100 $\mu\text{g}/\text{ml}$ (85 pM to 850 nM) interval so as to
13
14 perfectly match the range of the cardiovascular disease risk in blood assay adopted for clinical
15
16 diagnosis. This result demonstrates the flexibility of the sensor over different dynamic ranges. This
17
18 sensor is also endowed with full compatibility with silicon industrial technology, low cost, high
19
20 selectivity and rapid response. Moreover, by changing the functionalization the use of Si NW
21
22 sensors opens the route towards a new class of promising optical sensors for different application
23
24 fields.
25
26
27
28
29

30 **Experimental Section**

31 *Materials*

32
33
34 Streptavidin from *Streptomyces avidinii* and BSA were purchased by Sigma-Aldrich. Streptavidin-
35
36 Alexa Fluor[®] 488 fluorescent conjugate was obtained from ThermoFisher Scientific. The
37
38 biotinylated Anti-CRP (Ab) monoclonal antibody and the CRP protein from human plasma were
39
40 respectively purchased from HyTest and Scripps Laboratories.. High performance liquid
41
42 chromatography (HPLC)-grade water was purchased from Sigma-Aldrich. Phosphate-buffered
43
44 saline (PBS) buffer tablets were purchased from Sigma-Aldrich and PBS solution was prepared
45
46 yielding a 10 mM solution with pH 7.4.
47
48
49
50

51 *Fabrication of Si NW sensors*

52
53
54 Si NWs were produced by MACE starting from (100)-oriented n type doped (1.5-4 $\Omega\cdot\text{cm}$)
55
56 commercial Si wafers. Si substrates are first oxidized for 2 min by UV ozone treatment and
57
58
59
60

1
2
3 immersed in a 5% hydrofluoric acid (HF) solution for 5 min in order to obtain an oxide-free
4 silicon surface. A thin discontinuous layer of 2 nm of gold is deposited on the clean Si surface by
5 electron beam evaporation at room temperature in an ultra-high vacuum chamber. The Au deposited
6 Si wafer is then immersed in an etching aqueous solution of HF (5 M), H₂O₂ (0.44 M).
7
8

9
10
11 The deposited gold layer acts as catalyst, improving the local oxidization of the Si only underneath
12 the metal covered regions that are selectively etched by HF which causes the Au layer to sink into
13 the Si bulk, leading to the formation of thin NWs [42]. Unlike Vapor-Liquid-Solid (VLS)
14 mechanisms, each step of the process is performed at room temperature and the Au catalyst is
15 removed at the final process step by immersing the NW samples in a gold etchant solution for 1 min
16 [43].
17
18
19
20
21
22
23
24

25 Si NW sensors were fabricated by using the surface bio-functionalization procedure schematically
26 described in Figure 1a-c. The procedure starts with the as-grown Si NWs washing. To this end, the
27 NWs are immersed in an isopropanol bath for 2 min, rinsed in water for 2 min, treated with UV
28 cleaning for 5 min and rinsed in water for 2 min to remove any biological contamination from the Si
29 NWs surface. This procedure results also in the formation of a uniform layer of silicon oxide
30 surrounding the Si NWs. The presence of silicon dioxide increases the NWs surface hydrophilicity,
31 thus allowing a better diffusion of the bio-functionalization solutions within the NW interstices.
32 Moreover, it promotes a better physisorption of the SA proteins [44]. The bio-functionalization
33 performed afterwards involved the following steps: i) immersion in a SA solution for 16 hours
34 (Figure 1b) and ii) for 4 h incubation in a solution of biotinylated anti-CRP (Ab) specific for the
35 CRP binding (Figure 1c). Each functionalization step is performed at room temperature and
36 followed by three rinsing step in a phosphate buffer solution (PBS 10 mM, KCl 2.7 mM, 137 mM
37 NaCl, pH = 7.4) in order to remove the molecules not bound to the surface. The sample is finally
38 washed 3 times with HPLC grade water to rinse off salt buffer crystal residues on the surface and
39 then dried gently with nitrogen blow. To optimize the bio-functionalization process, different
40 concentrations of SA and Ab solution were investigated, always keeping at 1:5 the ratio between the
41
42
43
44
45
46
47
48
49
50
51
52
53
54
55
56
57
58
59
60

1
2
3 SA and Ab solutions concentrations. The large excess of Ab assures a complete saturation of all the
4
5 four linking sites of SA by the biotinylated anti-CRPs [37]. Specifically, a 1 $\mu\text{g/ml}$ of SA and 5
6
7 $\mu\text{g/ml}$ of Ab, a 10 $\mu\text{g/ml}$ of SA and 50 $\mu\text{g/ml}$ of Ab, and a 20 $\mu\text{g/ml}$ of SA and 100 $\mu\text{g/ml}$ of Ab,
8
9 where used. All solutions were prepared in PBS. The sensing measurements were performed by
10
11 incubating the bio-functionalized NWs for 4 hours at room temperature in CRP solutions at
12
13 different concentrations ranging from 10^{-9} to 100 $\mu\text{g/ml}$ (8.5 aM to 850 nM). Afterwards, they were
14
15 washed in PBS to remove the unreacted species, then rinsed with HPLC grade water and dried
16
17 under nitrogen blow. For the first negative control experiment, the SA (10 $\mu\text{g/mL}$ in PBS)
18
19 functionalized NWs were immersed in BSA solution (50 $\mu\text{g/mL}$ in PBS) instead of Ab. The other
20
21 control experiment was carried out by exposing the fully functionalized NWs (*i.e.* 10 $\mu\text{g/ml}$ of SA
22
23 and 50 $\mu\text{g/ml}$ of Ab) to different concentrations of BSA ranging from 10^{-5} $\mu\text{g/ml}$ to 10 $\mu\text{g/ml}$.
24
25
26
27 Incubation times and washing steps with PBS and HPLC grade water were kept the same as in case
28
29 of CRP.
30
31
32
33

34 *Si NW sensors structural and optical characterization*

35
36
37 NW structural characterizations were obtained by scanning electron microscopy (SEM) using a
38
39 field emission Zeiss Sigma microscope (5kV, 30 μm aperture). Fluorescence imaging of the samples
40
41 were performed by means of direct Laser Scanning Confocal Microscopy (LSCM) using the TCS
42
43 SP8 SMD confocal microscope by LEICA equipped with a white light and a blue diode laser
44
45 (excitation wavelength was 405 nm). A droplet (20 μL) of distilled water was deposited on the Si
46
47 NWs array. The just deposited water droplets are characterized by high contact angle but in a few
48
49 minutes the contact angle decreases and the droplet wets the Si NWs. At this point a clean cover
50
51 slip is pressed on the droplet to squeeze out the excess water leaving a continuous aqueous layer
52
53 that surrounds the NWs and is in contact with the cover slip itself. Samples were observed using a
54
55 x63 water-immersion lens. The emission of Si NWs is obtained by exciting the system with a diode
56
57
58
59
60

1
2
3 laser at 405 nm where NW absorption is maximized and then acquired in the 630-800 nm spectral
4
5 range, where the Alexa Fluor 488 contribution is negligible. In fact, in the 630-800 nm range the PL
6
7 peak of NWs is present, whereas the Alexa Fluor PL emission peak is limited in the 505-520 nm
8
9 range and its emission is close to zero in the 630-800 nm analyzed region. The fluorescence
10
11 emission from the labelled streptavidin deposited on Si NWs is obtained by exciting at 488 nm that
12
13 corresponds to the maximum of absorption for the Alexa Fluor through a white light. The emission
14
15 is then collected in the 505-520 nm spectral range. We verified that under these experimental
16
17 conditions the emission from NWs is not visible.
18
19

20 Photoluminescence (PL) measurements were performed by focusing the 364 nm line of an Ar⁺ laser
21
22 onto the sample through a UV fluorinated 60x objective (NA=0.9) at a laser power of about 80 μW
23
24 measured on the sample. PL spectra were acquired by a HR800 spectrometer (Horiba Jobin Yvon)
25
26 coupled to a cooled CCD detector. PL lifetime measurements were performed by exciting the
27
28 system to the steady state with the 488 nm line of an Ar⁺ laser at a power of 10 mW (chopped by an
29
30 acousto-optic modulator at a frequency of 55 Hz) and then monitoring the decay of the PL signal at
31
32 the detection wavelength of 700 nm through a phototube coupled to an oscilloscope.
33
34
35
36
37

38 **Acknowledgments**

39
40 We thank M. Magliulo and F. Iacona for useful discussions. G. Gismondo, R. Caruso, D. Arigò, G.
41
42 Lupò, G. Spinella and C. Percolla are acknowledged for expert technical assistance. PON
43
44 SISTEMA (MIUR) project is acknowledged for partial financial support. AI acknowledges the
45
46 project PON_00214_1 named TECLA.
47
48
49
50
51
52
53
54
55
56
57
58
59
60

References

1. Alivisatos, A. P. The Use Of Nanocrystals In Biological Detection. *Nature Biotechnology* **2003**, *22*, 47-52.
2. Ahn, C. H.; Choi, J.-W.; Beaucage, G.; Nevin, J. H.; Lee, J.-B.; Puntambekar, A.; Lee, R. Y. Disposable Smart Lab On A Chip For Point-Of-Care Clinical Diagnostics. *Proceedings of the IEEE* **2004**, *92*, 154-173.
3. Martinez, K.; Hart, J. K.; Ong, R. Environmental Sensor Networks. *IEEE Computer* **2004**, *37*, 50-56.
4. Duncan, T. Applications of Nanotechnology in Food Packaging and Food Safety: Barrier Materials, Antimicrobials and Sensors. *Journal of Colloid and Interface Science* **2011**, *363*, 1-24.
5. Gao, D.; Wang, Z.; Liu, B.; Ni, L.; Wu, M.; Zhang, Z. Resonance Energy Transfer-Amplifying Fluorescence Quenching at The Surface of Silica Nanoparticles Toward Ultrasensitive Detection of TNT. *Analytical Chemistry* **2008**, *80*, 8545-8553.
6. Yu, Y.; Chen, X.; Wei, Y.; Liu, J.; Yu, S.; Huang, X. Cdse Quantum Dots Enhance Electrical and Electrochemical Signals of Nanogap Devices for Bioanalysis. *Small* **2012**, *8*, 3274-3281.
7. Wang, J. Carbon-Nanotube Based Electrochemical Biosensors: A Review. *Electroanalysis* **2005**, *17*, 7-14.
8. Wanekaya, A.; Chen, W.; Myung, N.; Mulchandani, A. Nanowire-Based Electrochemical Biosensors. *Electroanalysis* **2006**, *18*, 533-550.
9. Patolsky, F.; Zheng, G.; Lieber, C. M. Fabrication of Silicon Nanowire Devices For Ultrasensitive, Label-Free, Real-Time Detection Of Biological And Chemical Species. *Nature Protocols* **2006**, *1*, 1711-1724.

10. Zheng, G.; Xuan, G. P. A.; Lieber, C. M. Frequency Domain Detection of Biomolecules Using Silicon Nanowire Biosensors. *Nano Lett.* **2010**, *10*, 3179–3183.
11. Zheng, G.; Lieber, C. M. Nanowire Biosensors for Label-Free, Real-Time, Ultrasensitive Protein Detection. *Methods in Molecular Biology* **2011**, 223-237.
12. Bunimovich, Y. L.; Shin, Y. S.; Yeo, W.; Amori, M.; Kwong, G.; Heath, J. R. Quantitative Real-Time Measurements of DNA Hybridization with Alkylated Nonoxidized Silicon Nanowires in Electrolyte Solution. *Journal of the American Chemical Society* **2006**, *128*, 16323-16331.
13. Cui, Y.; Wei Q.; Park, H.; Lieber, C. M. Nanowire Nanosensors for Highly Sensitive and Selective Detection of Biological and Chemical Species. *Science* **2001**, *293*, 1289-1292
14. Lequin, R. M. Enzyme Immunoassay (EIA)/Enzyme-Linked Immunosorbent Assay (ELISA). *Clinical Chemistry* **2005**, *51*, 2415-2418.
15. Gan, S. D.; Patel, K. R. Enzyme Immunoassay and Enzyme-Linked Immunosorbent Assay. *Journal of Investigative Dermatology* **2013**, *133*, 1-3.
16. Sapsford, K. E.; Pons, T.; Medintz, I. L.; Mattoussi, H. Biosensing with Luminescent Semiconductor Quantum Dots. *Sensors* **2006**, *6*, 925-953.
17. Alivisatos, A. P. Semiconductor Clusters, Nanocrystals, And Quantum Dots. *Science* **1996**, *271*, 933-937.
18. Dohnalová, K.; Poddubny, A. N.; Prokofiev, A. A.; de Boer, W. D. A.; Umesh, C. P.; Paulusse, J. M. J.; Zuilhof, H.; Gregorkiewicz, T. Surface Brightens Up Si Quantum Dots: Direct Bandgap-Like Size-Tunable Emission. *Light: Science & Applications* **2013**, *2*, e47.
19. Costa-Fernández, J. M.; Pereiro, R.; Sanz-Medel, A. The Use of Luminescent Quantum Dots for Optical Sensing. *TrAC Trends in Analytical Chemistry* **2006**, *25*, 207-218.
20. Punyadeera, C.; Dimeski, G.; Kostner, K.; Beyerlein, P.; Cooper-White, J. One-step homogeneous C-reactive protein assay for saliva. *Journal of Immunological Methods* **2011**, *373*, 19–25.

- 1
2
3 21. Zheng, G.; Patolsky, F.; Cui, Y.; Wang, W. U.; Lieber, C. M. Multiplexed electrical
4 detection of cancer markers with nanowire sensor arrays. *Nature Biotechnology* **2005**,
5 *23*,
6 1294-1301.
7
8
9
10 22. Zhao, X.; Tapecc-Dytioco, R.; Tan, W. Ultrasensitive DNA Detection Using Highly
11 Fluorescent Bioconjugated Nanoparticles. *Journal of American Chemistry Society* **2003**,
12 *125*, 11474-11475.
13
14
15
16 23. Sierks, M. R.; Chatterjee, G.; McGraw C.; Kasturirangan, S.; Schulz, P.; Prasad, S. CSF
17 levels of oligomeric alpha-synuclein and beta-amyloid as biomarkers for neurodegenerative
18 disease. *Integr. Biol.* **2011**,*3*,1188–1196.
19
20
21
22
23 24. An, J. H.; Choi, D.-K.; Lee, K.-J.; Choi, J.-W. Surface-enhanced Raman spectroscopy
24 detection of dopamine by DNA Targeting amplification assay in Parkisons's model.
25 *Biosensors and Bioelectronics* **2015**, *67*, 739–746.
26
27
28
29
30 25. Peng, Z. A.; Peng, X. Formation of High-Quality CdTe, CdSe, and CdS Nanocrystals Using
31 CdO as Precursor. *Journal of American Chemistry Society* **2001**, *123*, 183-184.
32
33
34 26. Zayats, M.; Kharitonov, A. b.; Pogorelova, S. P.; Lioubashevski, O.; Katz, E.; Willner, I.
35 Probing Photoelectrochemical Processes In Au–Cds Nanoparticle Arrays By Surface
36 Plasmon Resonance: Application For The Detection Of Acetylcholine Esterase
37 Inhibitors. *Journal of the American Chemical Society* **2003**, *125*, 16006-16014.
38
39
40
41
42
43 27. Irrera, A.; Pacifici, D.; Miritello, M.; Franzò, G.; Priolo, F.; Iacona, F.; Sanfilippo, D.; Di
44 Stefano, G.; Fallica, P. G. Excitation And De-Excitation Properties Of Silicon Quantum
45 Dots Under Electrical Pumping. *Applied Physics Letters* **2002**, *81*, 1866-1868.
46
47
48
49 28. Tischler, M. A.; Collins, R. T.; Stathis, J. H.; Tsang, J. C. Luminescence Degradation In
50 Porous Silicon. *Applied Physics Letters* **1992**, *60*, 639-641.
51
52
53
54 29. Priolo, F.; Gregorkiewicz, T.; Galli, M.; Krauss, T. F. Silicon Nanostructures for Photonics
55 and Photovoltaics. *Nature Nanotechnology* **2014**, *9*, 19-32.
56
57
58
59
60

- 1
2
3 30. Fabbri, F.; Rotunno, E.; Lazzarini, L.; Fukata, N.; Salviati, G. Visible And Infra-Red Light
4 Emission In Boron-Doped Wurtzite Silicon Nanowires. *Scientific Reports* **2014**, *4*,
5
6
7 31. Lo Faro, M. J.; D'Andrea, C.; Messina, E.; Fazio, B.; Musumeci, P.; Reitano, R.; Franzò,
8 G.; Gucciardi, P. G.; Vasi, C. S.; Priolo, F.; Iacona, F.; Irrera, A. Silicon nanowire and
9 carbon nanotube hybrid for room temperature multiwavelength light source. *Scientific*
10 *Reports* **2015**, *5*, 1-10.
11
12
13
14
15
16 32. Fazio, B.; Artoni, P.; Iatì, M. A.; D'Andrea, C.; Lo Faro, M. J.; Del Sorbo, S.; Pirotta, S.;
17 Gucciardi, P. G.; Musumeci, P.; Vasi, C. S.; Saija, R.; Galli, M.; Priolo, F.; Irrera, A.
18 Strongly enhanced light trapping in a two-dimensional silicon nanowire random fractal
19 array. *Light: Science & Applications* **2016**, *5*, e16062.
20
21
22
23
24
25 33. Fazio, B.; Irrera, A.; Pirotta, S.; D'Andrea, C.; Del Sorbo, S.; Lo Faro, M. J.; Gucciardi, P.
26 G.; Iatì, M. A.; Saija, R.; Patrini, M.; Musumeci, P.; Vasi, C. S.; Wiersma, D. S.; Galli, M.;
27 Priolo, F. Coherent backscattering of Raman light. *Nature Photonics* **2017**, *11*, 170–176.
28
29
30
31
32 34. Ridker, P. M.; Clinical Application of C-Reactive Protein for Cardiovascular Disease
33 Detection and Prevention. *Circulation* **2003**, *107*, 363-369.
34
35
36 35. Benjamin, E. J.; Blaha, M. J.; Chiuve, S. E.; Cushman, M.; Das, S. R.; Deo, R.; de Ferranti,
37 S. D.; Floyd, J.; Fornage, M.; Gillespie, C.; Isasi, C. R.; Jiménez, M. C.; Jordan, L. C.; Judd,
38 S. E.; Lackland, D.; Lichtman, J. H.; Lisabeth, L.; Liu, S.; Longenecker, C. T.; Mackey, R.
39 H.; et al. Heart Disease and Stroke Statistics—2017 Update: A Report From the American
40 Heart Association. *Circulation* **2017**, CIR.0000000000000485, e1-e459.
41
42
43
44
45
46
47 36. Algarra, M.; Gomes, D.; Esteves da Silva, J. C. Current analytical strategies for C-reactive
48 protein quantification in blood. *Clinica Chimica Acta* **2013**, *415*, 1–9.
49
50
51
52 37. Thermo Fisher Avidin-Biotin Technical Handbook. *Thermo Scientific*
53 <https://tools.thermofisher.com/content/sfs/brochures/1601675-Avidin-Biotin-Handbook.pdf>
54
55
56
57
58
59
60

- 1
2
3 38. Gesztelyi, R.; Zsuga, J.; Kemeny-Beke, A.; Varga, B.; Juhasz, B.; Tosaki A.; The Hill
4 equation and the origin of quantitative pharmacology. *Arch. Hist. Exact Sci.* **2012**, 66, 427-
5 438
6
7
8
9
10 39. Salazar, J.; Martínez, M. S.; Chávez, M.; Toledo, A.; Añez,R.; Torres, Y.; Apruzzese, V.;
11 Silva, C.; Rojas, J.; Bermúdez V.; C-Reactive Protein: Clinical and Epidemiological
12 Perspectives. *Cardiology Research and Practice* **2014**, 2014, 1-10.
13
14
15
16 40. Bayer, E. A.; Ben-Hur, H.; Hiller, Y.; Wilchek, M.; Postsecretory modifications of
17 streptavidin. *Biochem. Journal* **1989**, 259, 369-376.
18
19
20 41. Wu, S-C; Wong, S-L; Engineering Soluble Monomeric Streptavidin with Reversible Biotin
21 Binding Capability. *Journal of Biological Chemistry* **2005**, 280, 23225–23231.
22
23
24
25 42. Irrera, A.; Artoni, P.; Iacona, F.; Pecora, E. F.; Franzò, G.; Galli, M.; Fazio, B.; Boninelli,
26 S.; Priolo, F. Quantum Confinement and Electroluminescence in Ultrathin Silicon
27 Nanowires Fabricated by a Maskless Etching Technique. *Nanotechnology* **2012**, 23, 075204.
28
29
30 43. Irrera, A.; Lo Faro, M. J.; D’Andrea, C.; Leonardi, A. A.; Artoni, P.; Fazio, B.; Picca, R. A.;
31 Cioffi, N.; Trusso, S.; Franzò, G.; Musumeci, P.; Priolo, F.; Iacona, F.; Light-emitting
32 silicon nanowires obtained by metal-assisted chemical etching. *Semicond. Sci. Technol.*
33 **2017**, 32, 1-20.
34
35
36
37
38
39
40 44. Van Noort, D.; Welin-Klintström, S.; Arwin, H.; Zangoie, S.; Lundström I.; Mandenius,
41 C.-F.; Monitoring specific interaction of low molecular weight biomolecules on oxidized
42 porous silicon using ellipsometry. *Biosensors and Bioelectronics* **1998**, 13, 439-449.
43
44
45
46
47
48
49
50
51
52
53
54
55
56
57
58
59
60

Figure 1

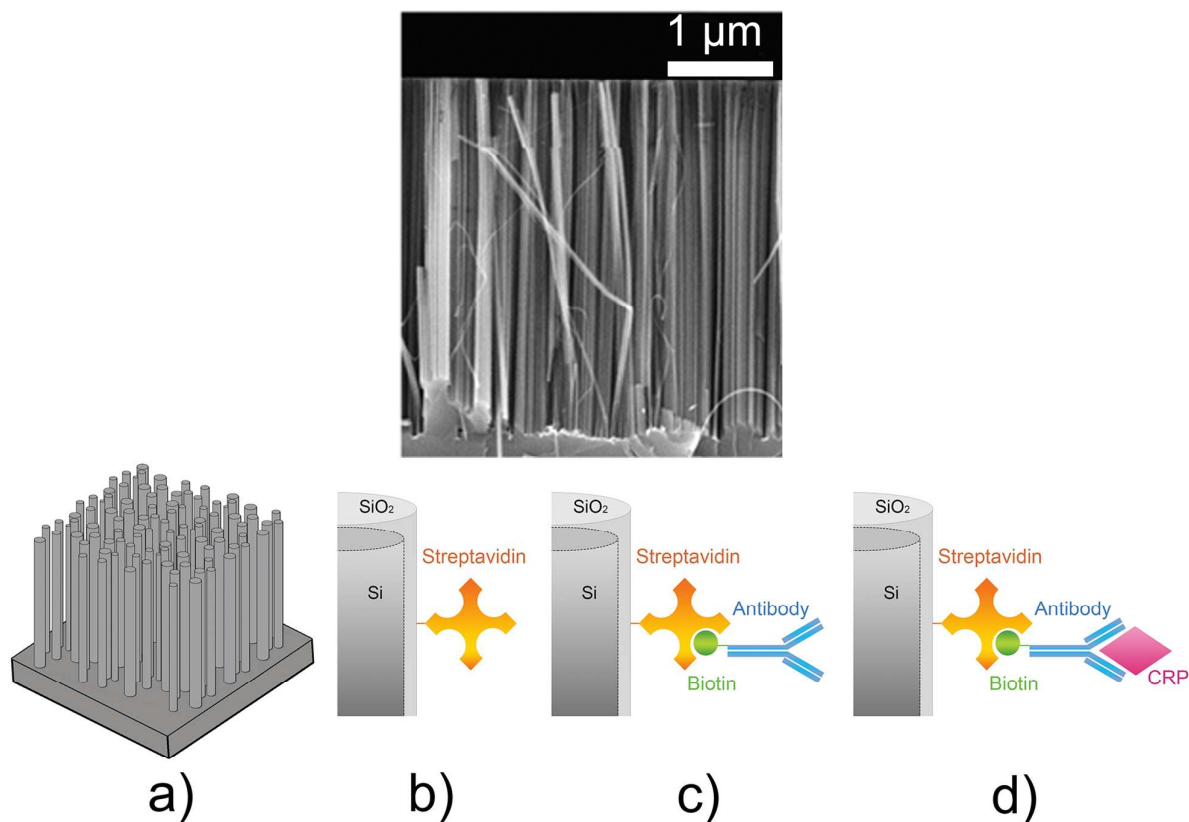


Figure 1. Cross section SEM image of Si NW array length of about 3 μm. Schematic illustration of the functionalization process: (a) NW array obtained by MACE, (b) functionalization of Si NW surface with streptavidin, (c) functionalization with the specific biotinylated antibody for CRP. (d) Capture of CRP due to the bioaffinity interaction with Ab.

Figure 2

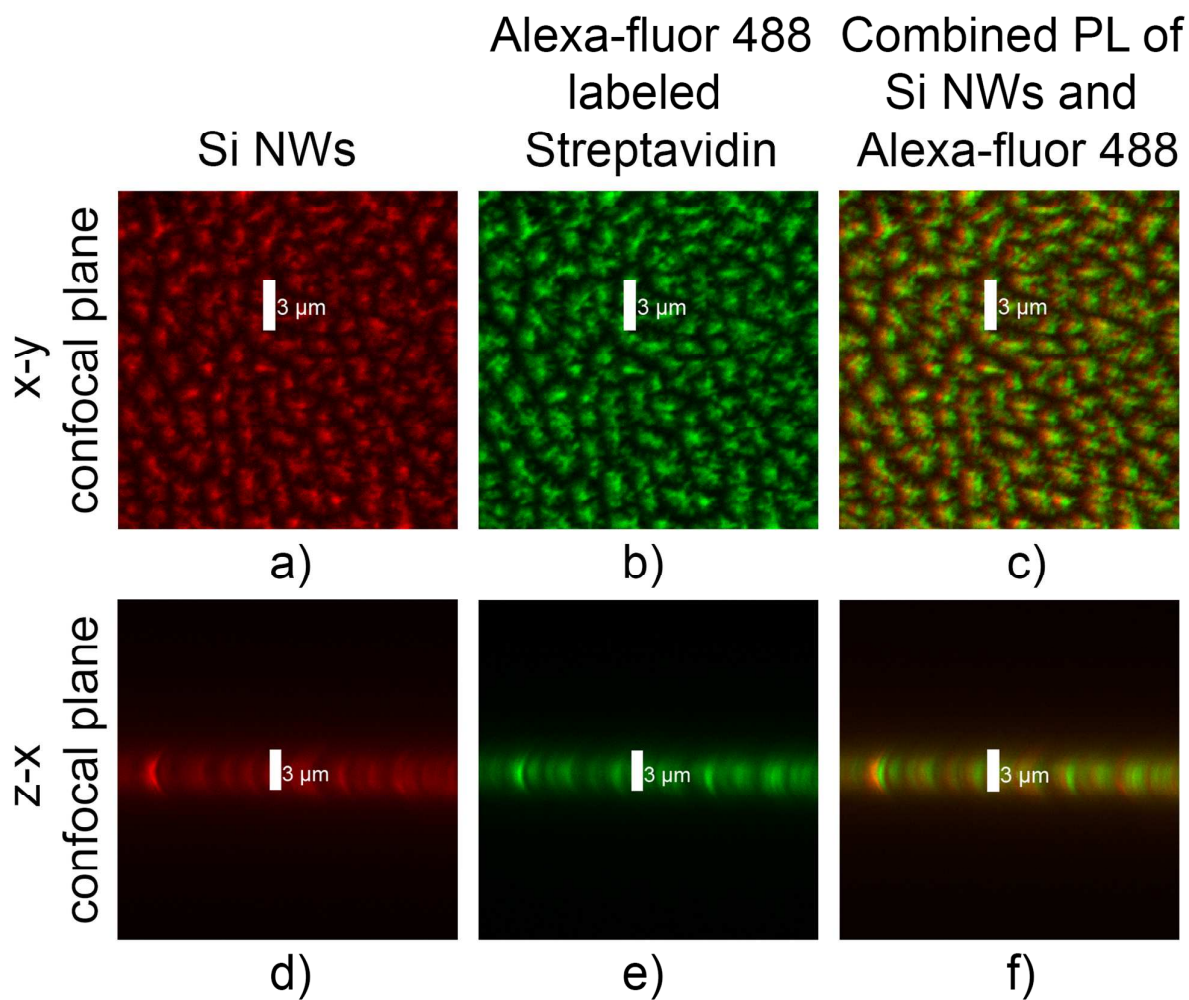


Figure 2. Confocal microscopies of a NW sample functionalized with Streptavidin bounded with Alexa fluor 488. The PL emission of only Si NWs is displayed in red (a) X-Y confocal plane and (b) Z-X confocal plane. The PL emission of only Alexa fluor 488 is reported in green (c) in X-Y confocal plane and (d) in Z-X confocal plane. Combination of the PL emission of Si NWs and ALEXA fluor 488 (e) in X-Y confocal plane and (f) in Z-X confocal plane.

Figure 3

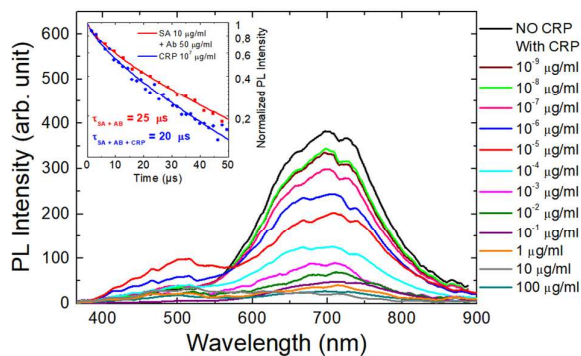


Figure 3. PL spectra of the NW sensor reported for different CRP concentrations and the PL reference sensor without CRP showed in black. The inset displays the PL lifetime of the reference without CRP (red squares) and of the sensor incubated with 10^{-7} $\mu\text{g/ml}$ of CRP (blue dots).

Figure 4

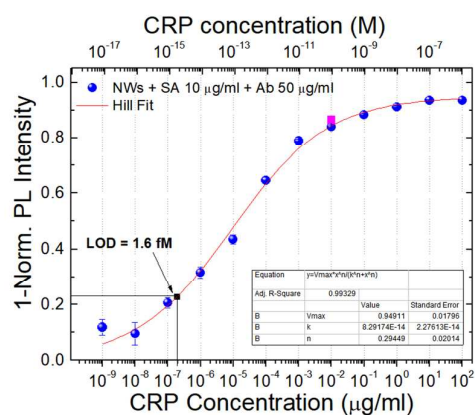


Figure 4. Trend of the sensor response as a function of the CRP concentration, normalized to the full quenching of the sensor. Red line is the Hill's binding model fit. Magenta point is the quenching value measured by a sensor immersed in human serum with 10^{-2} $\mu\text{g/ml}$ of CRP. The LODs 1.6 fM is marked in black in figure.

Figure 5

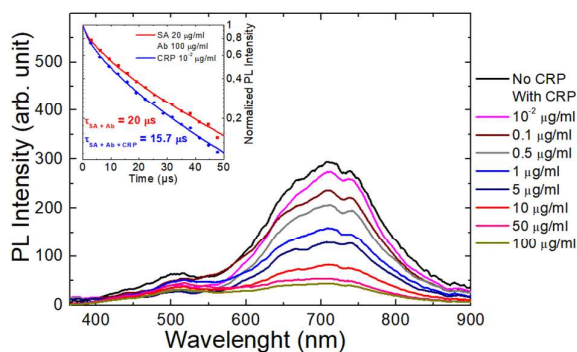


Figure 5. PL spectra of the NW sensor reported for different CRP concentrations and the PL reference sensor without CRP showed in black. The inset displays the PL lifetime of the reference without CRP (red squares) and of the sensor incubated with 10^{-2} $\mu\text{g/ml}$ of CRP (blue dots).

Figure 6

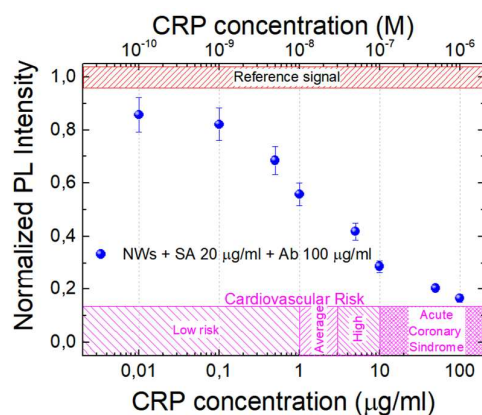


Figure 6. Trend of the PL integrated peak, normalized to the reference (red bar), as a function of the CRP concentration. In the figure (magenta) the CRP range concentration in human serum for cardiovascular risk is reported.

Figure 7

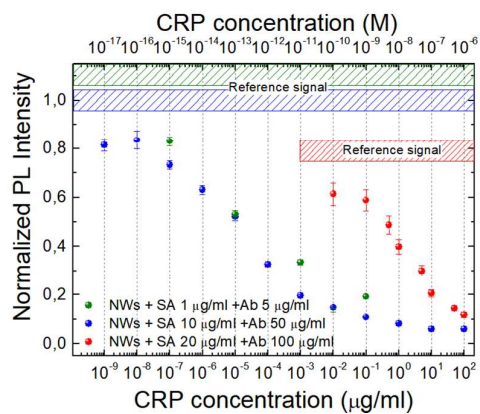


Figure 7. Trend of the integrated PL peak for SA1/Ab5 (green dots), SA10/Ab50 (blue dots) and SA20/Ab100 (red dots) normalized to their references as a function of the CRP concentration.